NANO EXPRESS

Ultraviolet Laser Action in Ferromagnetic $Zn_{1-x}Fe_xO$ Nanoneedles

H. Y. Yang · S. F. Yu · S. P. Lau · T. S. Herng · M. Tanemura

Abstract Fe-doped ZnO nanoneedles (NDs) were fabricated by an Ar^+ ion sputtering technique operated at room temperature. The as-grown samples show both ferromagnetic and lasing properties. The saturated magnetization moment was measured from 0.307 to 0.659 emu cm^{-3} at the field of 10 kOe with various Fe concentrations. Intense ultraviolet random lasing emission was observed from $Zn_{1-x}Fe_xO$ NDs at room temperature. The X-ray photoelectron spectroscopy result reveals that the doped Fe atoms occupy the Zn sites and lead to a decrease in oxygen deficiency.

Keywords $Zn_{1-x}Fe_xO$ · Nanoneedles · Ferromagnetic · Random lasing · Ion beam

ZnO-based diluted magnetic semiconductors (DMSs) have attracted great research attention due to a high Curie temperature above 300 K as predicted by theoretical calculation [1, 2]. Recently, ZnO-based DMSs bulk materials and thin films doped with Mn [3], Cu [4], Fe [5], and Co [6] have been realized by various fabrication methods. On the other hand, developing one-dimensional (1D) DMS materials are of great interest, for the reason that the 1D nanomaterials are ideal research systems for fabricating nanoscale field effect transistors, sensors, optoelectronic devices, logic circuits, and lasers [7]. Hence, 1D ZnO DMS material has been prepared by vapor–solid process and incorporation doping in the precursors [8–10]. However, these fabrication methods may lead to variance in environment of doping element in the matrix or forming second phase. Ideally, the combination of ferromagnetism and optical properties in 1D DMS material can open many new possibilities of freedom and functionality for the fabrication of unique nano-devices. Hence, few research groups have focused their investigation on the study of the photon luminance and stimulated emission from the DMS materials [11, 12]. Nevertheless, there is no report on the observation of the random lasing emissions from DMS materials.

In this letter, we established an effective fabrication method to realize 1D Fe-doped ZnO nanoneedles (NDs) which support random lasing action at ultraviolet (UV) wavelength. The surface morphology of an as-grown sample was characterized by scanning electron microscopy (SEM). X-ray diffraction (XRD) and transmission electron microscope (TEM) were also employed to investigate the crystallinity, which shows the Fe atoms have been doped into the ZnO lattice. Furthermore, the ferromagnetic and lasing properties of $Zn_{1-x}Fe_xO$ NDs have been investigated. The X-ray photoelectron spectroscopy (XPS) was used to find out the oxygen deficiency changing in the slightly doped $Zn_{1-x}Fe_xO$ NDs sample.

As shown in Fig. 1a, $Zn_{1-x}Fe_xO$ NDs were fabricated in ZnO thin films by an ion-beam system. The fabrication procedures are similar to ZnO NDs which have been reported elsewhere [13]. In brief, 400 nm-ZnO thin films are deposited on SiO_2/Si substrate by a filtered cathodic

H. Y. Yang (✉) · S. F. Yu · T. S. Herng
School of Electrical and Electronic Engineering, Nanyang Technological University, Nanyang 639798, Singapore
e-mail: hyyang@ntu.edu.sg

S. P. Lau
Department of Applied Physics, The Hong Kong Polytechnic University, Hung Hom, Kowloon, Hong Kong

M. Tanemura
Graduate School of Engineering, Nagoya Institute of Technology, Gokiso-Cho, Showa-Ku, Nagoya 466-8555, Japan

Fig. 1 **a** The geometrical configuration of ion-beams sputtering and Fe doping process. **b** XRD results of as-synthesized sample. **c** SEM images of $Zn_{0.989}Fe_{0.011}O$ NDs. **d** TEM image of a single $Zn_{0.989}Fe_{0.011}O$ nanoneedle. **e** High-resolution TEM image of the nanoneedle and **f** the corresponding selected area electron diffraction pattern
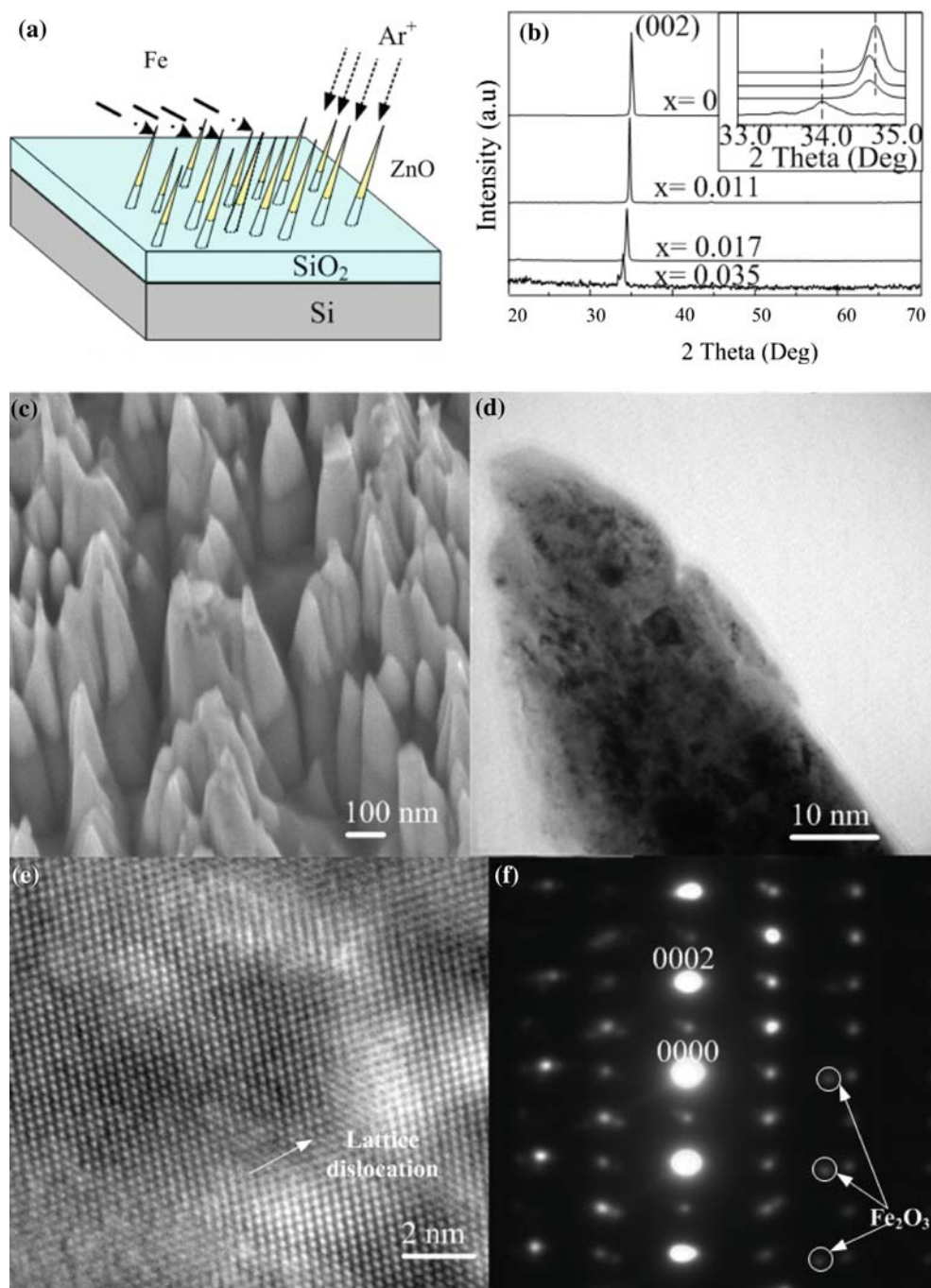
vacuum arc (FCVA) technique at 200 °C. 3 keV Ar^+ ions were focused into a microbeam with 380 μm in diameter for sputtering the thin films in a vacuum reaction chamber. At the same time, an arc plasma gun with Fe ion source was operated in pulse modes at 0.2, 0.5, and 1.0 Hz to dope Fe atom in the new forming ZnO NDs, and the corresponding Fe content in the $Zn_{1-x}Fe_xO$ NDs was estimated to be ~1.1, 1.7 and 3.5 at. %, respectively, by the XPS analysis. Figure 1b shows the XRD θ–2θ scan of the as-grown samples. It is found that only (002) reflections were

detected, which confirmed c-axis dominated structure of the samples. No secondary phase was found from the XRD spectrum, which indicated that the doping Fe must be incorporated into the lattice as substitution atom. However, for $Zn_{0.965}Fe_{0.035}O$ sample, clear decreases of intensity and increase in FWHM of the XRD peaks were detected. These results implied that when $x \geq 0.035$, the crystal-quality of the $Zn_{1-x}Fe_xO$ sample has decreased dramatically, even though there is no formation of secondary phase and precipitates in this doping concentration. An expansion in

lattice constant can be also seen from the XRD spectrum, the corresponding lattice expansion is calculated from the peak shift as $\Delta c/c = 2.43\%$ in the 3.5% Fe-doped sample.

Figure 1c shows the high magnification SEM image of as-deposited $Zn_{0.989}Fe_{0.011}O$ nanoneedle arrays with sharp-tip morphology. The diameter and length of the NDs are in the order of ~ 100 and 600 nm, respectively. It can be seen that the separation between the NDs was irregular and ranged from a few nanometers to tens of nanometers. As the ZnO thin film was only 400 nm thick, the upper part of the cone was $Zn_{0.989}Fe_{0.011}O$ (black contrast) and the lower part of the stem was SiO_2. A cross-sectional TEM image of a single $Zn_{0.989}Fe_{0.011}O$ nanoneedle (Fig. 1d), high-resolution TEM image (Fig. 1e) and the corresponding selective area electron diffraction (SAED) pattern (Fig. 1f) are exemplified to illustrate the crystal-quality of the $Zn_{0.989}Fe_{0.011}O$ NDs. The SAED pattern of the NDs is matched with the simulated ZnO pattern, implying that the nanoneedle exhibited the ZnO wurtzite structure. However, some weak diffraction spots of Fe_2O_3 could be seen in the pattern. Lattice distortion can also be observed in Fig. 1e. This is primarily due to the lattice constant mismatch between ZnO and the secondary phases (Fe_2O_3) as they have different crystal structures. These TEM results further illustrate the existence of the Fe element in the ZnO lattice which results to the ferromagnetism in ZnO NDs (Fig. 2).

In order to analyze the Fe doping of prepared sample, we measured the magnetization versus applied magnetic field curves for the $Zn_{1-x}Fe_xO$ NDs at with different compositions. The measurement was done 300 K by an alternating gradient magnetometer with a maximum field of 10 kOe. The $Zn_{1-x}Fe_xO$ NDs exhibit saturated room temperature magnetic moment (M_s) of 0.29, 0.37, and 0.66 emu g^{-1} with the Fe concentration as 1.1, 1.7, and 3.5 at.%, respectively. The well-defined hysteresis loops with coercive fields (H_c) of ~ 75, 97, and 275 Oe in these three samples implying the ferromagnetic properties at room temperature. These trends with doping concentration have been plot in the insert.

Investigations of the optical characteristics of the $Zn_{1-x}Fe_xO$ NDs samples were carried out by a 355 nm frequency–tripled Nd: YAG (10 Hz, 6 ns) pulse laser. Figure 3a, b, and c show the lasing spectra of the undoped ZnO, $Zn_{0.989}Fe_{0.011}O$, and $Zn_{0.983}Fe_{0.017}O$ NDs, respectively, as a function of optical excitation. When the pump power reached the threshold, Ith, a dramatic emission oscillation in a linewidth as narrow as 0.4 nm emerged from the single-broad emission spectra. Multiple laser modes with strong coherent feedback at wavelengths at the center wavelength ~ 394 nm (i.e., ZnO NDs), ~ 398 nm ($Zn_{0.989}Fe_{0.011}O$ NDs), and ~ 405 nm ($Zn_{0.983}Fe_{0.017}O$ NDs) were detected from these three NDs samples at room temperature. These lasing characteristics detected from all these NDs samples are in good agreements with our previous observation [14], which are due to random laser action. It should be also noted here, no lasing emission can be detected from $Zn_{0.965}Fe_{0.035}O$ sample even under a pumping intensity as high as ~ 1.6 MW cm^{-2}, which is expected due to the significant lattice deformation in this sample (i.e., shown from XRD results). A redshift up to ~ 11 nm was found in the emission wavelength. This kind of redshift in optical properties was also found in Co-doped

Fig. 2 Magnetization hysteresis loops of $Zn_{1-x}Fe_xO$ NDs at 300 K. *Insert* shows the saturated magnetization (M_s) and magnetic ordering with coercivity (H_c) as a function of Fe concentration
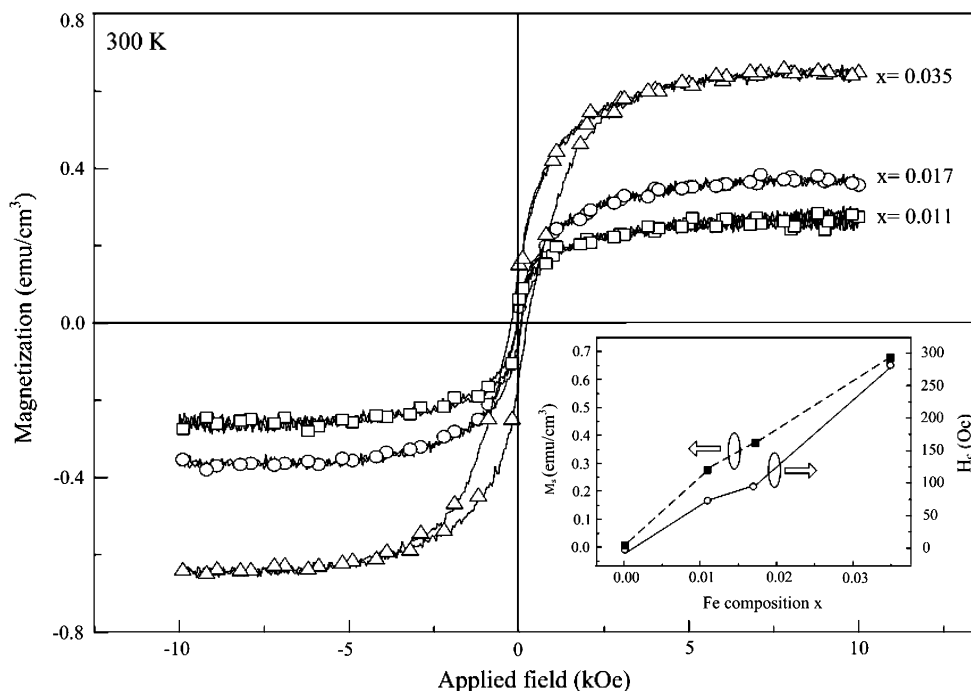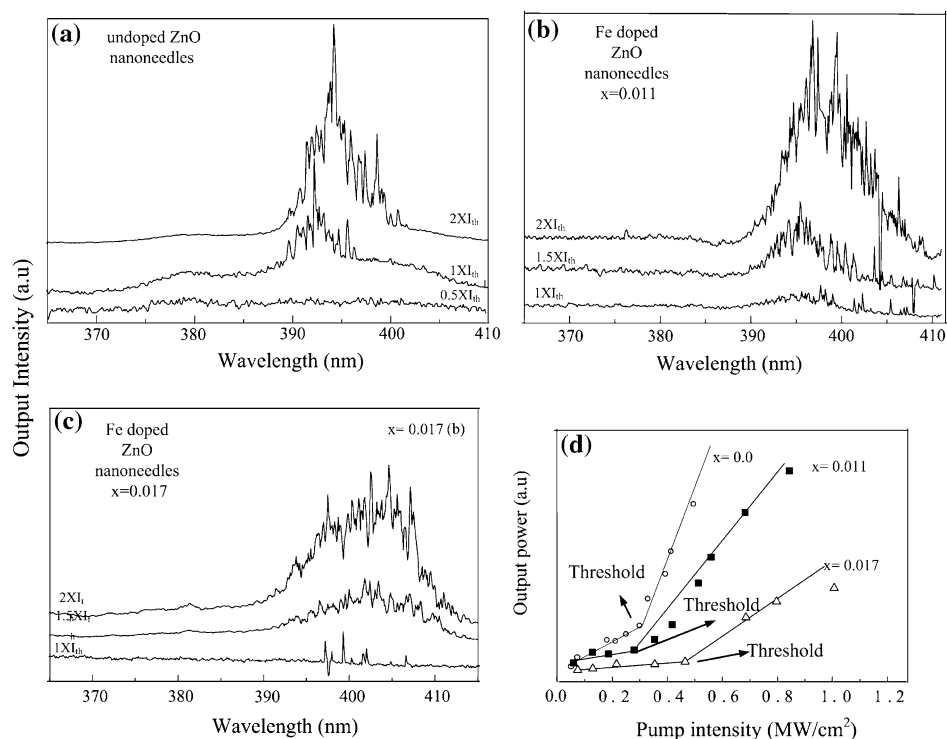
Fig. 3 Lasing emission spectra obtained from **a** undoped ZnO NDs, **b** $Zn_{0.989}Fe_{0.011}O$ NDs, and **c** $Zn_{0.983}Fe_{0.017}O$ NDs under different pumping density where the *I*th represents the lasing threshold. **d** Light–light curves of the undoped ZnO, $Zn_{0.989}Fe_{0.011}O$, and $Zn_{0.983}Fe_{0.017}O$ NDs

ZnO thin films [15]. The reason was proposed as that the *sp-d* exchange interactions between band electrons and localized *d* electrons of the Co^{2+} ions substituting for Zn ions. The redshift in our Fe-doped ZnO samples may also due to this reason. The electrons interchange give rise to a negative and a positive correction to the conduction- and valence-band edges, which lead to shrinkage of the band gap [16, 17].

Figure 3d shows the plots of emission intensity versus pumping intensity (i.e., light–light curve) of undoped ZnO, $Zn_{0.989}Fe_{0.011}O$, and $Zn_{0.983}Fe_{0.017}O$ NDs, respectively. Remarkably, it shows that the lasing threshold is decreased with slightly doped sample (i.e., $x = 0.011$), whereas increase to ~ 0.47 MW cm^{-2} when x increase to 0.017. It is known that the incorporation of 3*d* transition ions, such as Fe, generally deteriorates the crystallinity of ZnO due to their low solubility and various valence states [18], which is the mean reason for the increase of lasing threshold in the $Zn_{0.983}Fe_{0.017}O$ sample. This also suggested the increase in optical properties of $Zn_{0.989}Fe_{0.011}O$ sample. Hence, the slightly doped Fe can improve the crystallinity of undoped ZnO NDs. To compare the defects in the lattice of slightly Fe-doped ZnO and undoped ZnO NDs, we carryout XPS analysis for these two samples.

Figure 4 shows the XPS results from undoped and Fe-doped ZnO NDs. It was found that the chemical shift and signal intensity of Zn 2p$_{1/2}$ and Zn 2p$_{3/2}$ (data not shown) are similar in all these samples. The XPS data of $Zn_{0.989}Fe_{0.011}O$ NDs are shown in Fig. 4a. The insert figure

shows the Fe 2p$_{1/2}$ and Fe 2p$_{3/2}$ peaks located at 724.9 and 710.5 eV, respectively. Figure 4b, c, and d demonstrate O 1s peak and its deconvolution results for undoped ZnO and Fe-doped NDs. The deconvolution of peak was performed using a Gaussian distribution. According to literature, there are three types of oxygen energy levels existing in ZnO samples, i.e., O^{2-} of oxygen deficiency (i.e., 529.3 eV), O^{2-} in ZnO structure (i.e., 531.6 eV), and the chemically absorbed oxygen site (i.e., 534.1 eV) [19–21]. Although the Fe-doped ZnO NDs exhibited a slightly higher O 1s binding energy (i.e., 532.2 and 531.8 eV), the O^{2-} in $Zn_{0.989}Fe_{0.011}O$ structure has a similar amount of signal compare to undoped ZnO NDs. However, a significant reduction in the signal for oxygen deficiencies (~ 529.3 eV) was found in the slightly doped NDs. It is strongly implied that Fe is selectively bonded to electrons in singly ionized oxygen vacancies, which may increase the crystallinity of the sample. It has been reported that the Fe ions bonded to electrons can also reduce the chance of recombination of the electrons and photoexcited holes in the valence band [19, 22], which can deduce the green emission results from the recombination of electrons in singly ionized oxygen vacancies and photoexcited holes. Consequently, slightly doping of Fe into ZnO nanostructures decreased the oxygen deficiency, which results in the improvement of optical properties.

In summary, we have demonstrated successfully the in situ dope of Fe into ZnO NDs by ion sputtering method. Ferromagnetic characteristics of the Fe-doped ZnO NDs

Fig. 4 a XPS spectra of $Zn_{0.989}Fe_{0.011}O$ NDs, the *insert* shows the Fe 2p XPS core-level spectra; O 1s XPS core-level spectra of **b** undoped ZnO NDs, **c** $Zn_{0.989}Fe_{0.011}O$ NDs, and **d** $Zn_{0.983}Fe_{0.017}O$ NDs
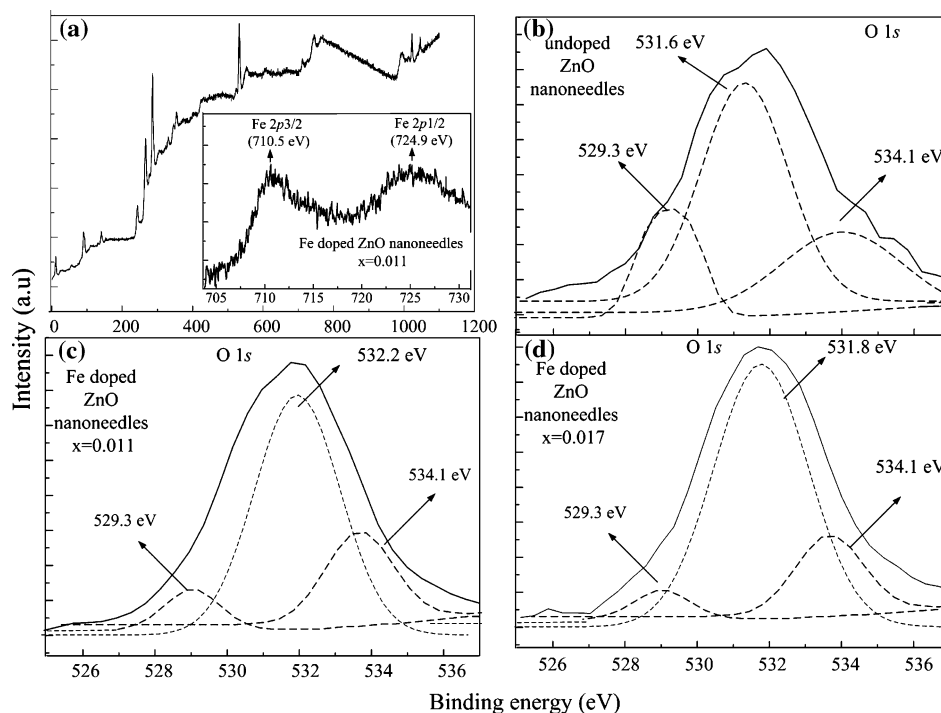
have been observed at room temperature. The UV lasing emissions from these magnetic NDs were also investigated. XPS measurements showed that oxygen deficiencies can be significantly reduced by slightly Fe doping in ZnO NDs. By combining magnetic and lasing functionality, these Fe-doped ZnO NDs have high potential to be used in variety of short wavelength optical devices, such as spin-polarized light emitters, spin-laser diodes, and optical switches and modulators.

References

1. S.A. Wolf, D.D. Awschalom, R.A. Buhrman, J.M. Daughton, S. von Molnár, M.L. Roukes, A.Y. Chtchelkanova, D.M. Treger, Science **294**, 1488 (2000)
2. T. Dietl, H. Ohno, F. Matsukura, J. Cibert, D. Ferrand, Science **287**, 1019 (2000)
3. Z. Yang, J.L. Liu, M. Biasini, W.P. Beyermann, Appl. Phys. Lett. **92**, 042111 (2008)
4. T.S. Herng, S.P. Lau, S.F. Yu, H.Y. Yang, X.H. Ji, J.S. Chen, N. Yasui, H. Inaba, J. Appl. Phys. **99**, 086101 (2006)
5. A.J. Chen, X.M. Wu, Z.D. Sha, L.J. Zhuge, Y.D. Meng, J. Phys. D Appl. Phys. **39**, 4762 (2006)
6. J.M. Baik, J.L. Lee, Adv. Mater. **17**, 2745 (2005)
7. Z.L. Wang, Adv. Mater. **19**, 889 (2007)
8. C.X. Xu, X.W. Sun, Z.L. Dong, M.B. Yu, Y.Z. Xiong, J.S. Chen, Appl. Phys. Lett. **86**, 173110 (2005)
9. X.M. Zhang, Y. Zhang, Z.L. Wang, W.J. Mai, Y.D. Gu, W.S. Chu, Z.Y. Wu, Appl. Phys. Lett. **92**, 162102 (2008)
10. J.J. Liu, M.H. Yu, W.L. Zhou, Appl. Phys. Lett. **87**, 172505 (2005)
11. J. Antony, S. Pendyala, A. Sharma, X.B. Chen, J. Morrison, L. Bergman, Y. Qiang, J. Appl. Phys. **97**, 10D307 (2005)
12. C. Ronning, P.X. Gao, Y. Ding, Z.L. Wang, D. Schwen, Appl. Phys. Lett. **84**, 783 (2004)
13. S.P. Lau, H.Y. Yang, S.F. Yu, H.D. Li, M. Tanemura, T. Okita, H. Hatano, H.H. Hng, Appl. Phys. Lett. **87**, 013104 (2005)
14. S.P. Lau, H.Y. Yang, S.F. Yu, C. Yuen, E.S.P. Leong, H.D. Li, H.H. Hng, Small **1**, 956 (2005)
15. M. Tay, Y.H. Wu, G.C. Han, T.C. Chong, Y.K. Zheng, S.J. Wang, Y.B. Chen, X.Q. Pan, J. Appl. Phys. **100**, 063910 (2006)
16. K.J. Kim, Y.R. Park, Appl. Phys. Lett. **81**, 1420 (2002)
17. Y.Z. Yoo, J. Appl. Phys. **90**, 4246 (2001)
18. T.S. Herng, S.P. Lau, S.F. Yu, H.Y. Yang, L. Wang, M. Tanemura, J.S. Chen, Appl. Phys. Lett. **90**, 032509 (2007)
19. S.H. Baek, J.J. Song, S.W. Lim, Physica B Condens. Matt. **339**, 101 (2007)
20. M.N. Islam, T.B. Ghosh, K.L. Chopra, H.N. Acharya, Thin Solid Films **280**, 20 (1996)
21. M. Chen, X. Wang, Y.H. Yu, Z.L. Pei, X.D. Bai, C. Sun, R.F. Huang, L.S. Wen, Appl. Surf. Sci. **158**, 134 (2000)
22. K. Vanheusden, C.H. Seager, W.L. Warren, D.R. Tallant, J.A. Voigt, Appl. Phys. Lett. **68**, 403 (1996)